Intracellular delivery of mRNA to human primary T cells with microfluidic vortex shedding

Amy A. Twite[1], Katherine H. W. J. Lau[1], Moein N. Kashani[1,2,3], Craig Priest[2,3], Jorge Nieva[1,4], David Gottlieb[1,5] and Ryan S. Pawell[1]

1. Indee Labs, 626 Bancroft Way, Suite A, Berkeley CA 94710, United States, E-mail: hello@indeelabs.com
2. Australian National Fabrication Facility, South Australia Node, Mawson Lakes SA 5095, Australia
3. Future Industries Institute, University of South Australia, Mawson Lakes SA 5095, Australia
4. Norris Cancer Center, University of Southern California, Los Angeles CA 90033, United States
5. University of Sydney, Sydney NSW 2006, Australia

Abstract

Intracellular delivery is a critical process in biology and medicine. During intracellular delivery, different constructs (e.g., functional macromolecules such as DNA, RNA, and protein, and various complexes) are delivered across the cell membrane and into the cytosol. Herein, we use a microfluidic post array to induce hydrodynamic conditions for cell membrane poration with microfluidic vortex shedding (*μVS*). *μVS* is then used for the intracellular delivery of mRNA to primary human pan T cells. The specific microfluidic device and experimental rig used in this study contains a 960 μm wide by 40 μm deep flow cell capable of processing more than 2 x 10^6 cells s^{-1} at volumes ranging from 100 μL to 1.5 mL. Furthermore, we demonstrate efficient enhanced green fluorescent protein (EGFP) mRNA expression (e.g., 57.4 ± 6.8% of viable, recovery cells, mean ± stdev) after mRNA delivery to human pan T cells with high cell viability (e.g., 83.7 ± 0.7% of recovered cells) and high cell recovery (e.g., 96.3 ± 1.1% of processed cells), resulting in net yield of 46.3 ± 5.6% viable, recovered, and GFP expressing human pan T cells at mRNA concentrations of 80 μg ml^{-1}. We also demonstrate *μVS* does not alter human pan T cell growth nor activation. These results demonstrated that *μVS* is a rapid intracellular delivery platform with promising potential for cytosolic delivery of mRNA to human primary T cells for (1) clinical applications, where larger volumes of cells are required and demonstrated value for (2) research applications, where rapid screening and minimal reagent consumption is preferable.

1. Introduction

Biomicrofluidics have been used to separate or enrich [1], modify[2], culture[3] and qualify[4] cells. Thus, biomicrofluidics lends itself to gene-modified cell therapy (GMCT) development and manufacturing where cells need to be separated or enriched, modified, cultured, and qualified. GMCTs based on modified T cells can provide substantially improved outcomes for patients with some hematological malignancies[5]. Specifically, chimeric antigen receptor T cell (CAR-T) therapies targeting CD19 have demonstrated remarkable responses and possibly cures in patients

with advanced acute lymphoblastic leukemia (ALL) that were unresponsive to all prior therapies. Gene modified CAR-T cells are the first cellular therapy to gain FDA approval for treatment of cancer following demonstration of an 83% remission rate in ALL[6].

CAR-T cells are generated via genetic modification of human T cells to display an extracellular antibody single-chain variable fragment (scFv) linked to a hinge region, one or more costimulatory domain(s), and an intracellular activating domain. The current standard of manufacture of these therapies using viral mediated gene transfer is costly, time consuming with relatively low throughput, and can have variable results depending on the cell type being modified[7–9]. In addition, the most problematic step in GMCT manufacturing is the intracellular delivery of nucleic acids via transfection or transduction for expression of the CAR by the T cell. Viral transduction using lentiviruses is the main method currently used to generate CAR-T therapies for clinical trial. However, these methods require significant hands-on time during production and require extensive intra- and post-production safety testing to avoid infusion of replication competent viruses at the time of therapy administration [7,10].

Physical transfection methods, such as electroporation, are appealing alternatives for GMCT manufacturing[2,11]. Electroporation does not require extensive safety or release precautions and can be used to deliver a broad range of constructs into cells (e.g. DNA, RNA, proteins and/or various complexes), but can result in significant cell losses or alteration of normal cell function[12,13]. Many alternative physical delivery methods to address these issues are currently in development. In general, microfluidic methods improve upon macroscale methods due to more uniform processing conditions—cell diameters and microfluidic channel geometries are on the same order of magnitude[14]. Examples of physical microfluidic intracellular delivery methods include flow through electroporation[15–17], microinjection[18], cell constriction or squeezing[19–24], fluid shear[14,25] and electrosonic jet ejection[26]. Though these methods offer promising and appealing alternatives to current GMCT, their production is limited by throughput, processing speeds, clogging, or lack of ease of translation from a research platform to clinical production.

Post arrays have been used for microfluidic transfection platforms to induce pore formation via mechanical deformation for cell models[19–22,24]. When cells pass through a constriction smaller than the diameter of the cell, mechanical deformation occurs resulting in the formation of temporary holes in the membrane. Han, X. *et al.* used microfluidic post arrays with spacing significantly larger than the cell diameter to add structural support to the long channel and disperse or scatter cells before they reach the deformation and transfection zone, where pores are formed via cell constriction through 4 μm wide spaces between posts[21]. Thus far, no example of microfluidic mechanical poration and transfection has been shown when coupling (1) post with a gap greater than cell diameter and (2) hydrodynamic conditions induced by μVS through a post array. While these examples have resulted in high transfection efficiency and post processing recovery, the constriction platform limits the amount of cell solution processed per device volume and limits flowrates (0.25 mL min^{-1} max for Han, X. *et al.*)[21]. This in turn reduces processing speeds while increasing clogging, which greatly limits the therapeutic yield of these platforms. Moreover, many studies using alternative mechanical poration methods are frequently restricted to cell models. Studies that do evaluate intracellular delivery to human primary T cells do not assess phenotype-specific delivery distribution or T cell activation[22,25,27]. Furthermore, the novel coupling of (1) a gap greater than the cell diameter and (2) hydrodynamic conditions is shown to not perturb human

primary T cells with respect to growth and activation while also being more flexible given that individual cell diameters within cell populations are not uniform.

The ideal intracellular delivery method for generation of GMCTs like CAR-T cells must be flexible across different constructs and applicable to a variety of cell types with minimal perturbation of cell viability, recovery and normal cell function. Currently, immune cells are being modified with plasmids[11,28], RNAs[29,30], and Cas9 ribonucleoprotein complexes (RNPs) [21,31] for generation of GMCTs. RNA is of particular interest as it offers significant utility with a range of modification modalities after intracellular delivery to T cells. This includes constructs to engineer immune cells in a permanent[28,31], long lived [27,32], or transient manner[29,30].

There are several practical metrics when considering microfluidic and physical intracellular delivery for GMCT development and manufacturing, including (1) cell recovery, (2) cell viability, (3) delivery or expression efficiency, (4) throughput, and (5) maintenance of normal or desired cell state and function. Low cell recovery rates are not ideal due to the large number of cells required for GMCTs. High cell viability is also essential as cells are frequently expanded after modification and low cell viability or the presence of dead cells is known to reduce cell growth rates. Additionally, nonviable cells can induce adverse immune response[33]. Regulators require a minimum percentage of viable cells for cell therapies as low cell viability at the time of administration can induce infusion toxicity and lessened therapeutic effect[34,35]. Delivery should induce a therapeutic effect without altering cell state, and efficiency of cell modification needs to be sufficiently high to avoid the need for additional processing steps like dead cell removal. Zhang *et al.* used electroporation to transfect naïve T cells with plasmids and found recovery rates to be less than 20% after 24 hours[12]. In addition to greatly reducing viability, electroporation increased expression of T cell surface activation markers, which requires additional post transfection recovery time before therapy administration[12]. Total throughput is as important as the rate at which cells can be processed–it is unlikely that single cell micro-needle injection[18] will be useful for GMCT manufacturing as generating the 10^8 cells without expansion requires up to 10^8 seconds, or approximately 3 years, to deliver perfect recovery, viability, and efficiency. Cumulatively, the current state of the art of microfluidic and physical intracellular delivery methods described above do not meet or exceed all the needs of GMCT development and manufacturing.

Microfluidics are being used to actively improve upon traditional intracellular delivery methods[24,36]. However, a substantial need for a practical microfluidic intracellular delivery method remains, particularly within the scope of GMCT development and manufacturing. Herein, we detail a hydrodynamic intracellular delivery method based on *μVS* (shown in Figure 1 a-e), along with its optimization for enhanced green fluorescent protein (EGFP) mRNA delivery to human pan T cells. We demonstrate *μVS* results in high cell recovery (e.g., 96.3 ± 1.1%, mean ± stdev), high cell viability (e.g., 83.7 ± 0.7%) and high EGFP expression efficiency (e.g., 57.4 ± 6.8%) resulting a yield of 46.3 ± 5.6% recovered, viable, and EGFP expressing pan T cells after intracellular delivery. We also demonstrate:

1. *μVS* does not adversely affect T cell growth.
2. *μVS* results in even EGFP expression profiles amongst T cell types.
3. *μVS* does not change T cell activation profiles.

This small-scale prototype also allows for processing rates of over 2 x 10^6 cells s^{-1} Finally, this prototype is fabricated with industry-standard semiconductor processes resulting in scalable device manufacturing with high yield (e.g., greater than 95%) and tight tolerances (e.g., less than 5%).

2. Methods

2.1. Device Design & Fabrication

Devices were designed with a 4.8 mm x 9.8 mm footprint and contained a 960 µm wide by a 40 µm deep flow cell. This flow cell contained a post array consisting of 40 µm diameter posts, with a pitch or distance between the midpoint of two adjacent posts in a post row of 60 µm orthogonal to the bulk flow direction, and a 500 µm pitch in the bulk flow direction. An overview of the device is shown in Figure 1g,h.

Device fabrication was achieved using industry standard semiconductor processes (Australian National Fabrication Facility, South Australia Node) and fused silica wafers. The flow cell and array geometries were constructed through anisotropic deep reactive ion etching (see Figure 1h). Deep reactive ion etched flow cells were thermally bonded to a fused silica lid containing 700 µm diameter laser machined through holes for the inlet and outlet. After fabrication, device and feature geometries were verified using scanning electron microscopy (see Figure 1h), white-light interferometry (not shown) and digital microscopy (not shown). Specific details on device design and fabrication are listed in the SI.

2.2. Experimental Rig Development

A purpose-built experimental rig was developed to operate a microfluidic chip using an operating pressure between 0 and 150 psig and measure flow rates ranging from 1 mL min^{-1} to 1 mL s^{-1}. To accomplish this, a compressed nitrogen tank was regulated down to less than 150 psig using a calibrated two-stage regulator and filtered down to 5 µm using a compressed air filter (McMaster Carr, 4414K71). Compressed nitrogen flow was then controlled with a manual on/off valve (McMaster Carr, 4379K61) and volumetric flow rates were measured with a calibrated mass flow meter (Alicat Scientific, M-1SLPM-D). Compressed nitrogen was then used to pneumatically drive samples of suspended cells and constructs through the microfluidic chip. The samples are housed in a 1.5 mL Eppendorf tube and placed in a tube adaptor (Elveflow, KRXS) which was coupled to an in-house fixture with outlet tubing for sample collection as seen in Figure 1f. More details regarding rig and device development, fabrication, and production are available in the SI section.

Non-dimensional equations were used to calculate the Reynolds number (*Re*) in channels and for flow around a cylindrical post[37]. This was done to determine if the post arrays were operating in the hydrodynamic or vortex shedding regime ($Re_o > 40$) while also determining if hydrodynamic conditions could be a result of flow through both the channel and the gap. The equations are based on the device's volumetric flow rate (Q), kinematic viscosity of the fluid (v) and specific device geometries. Using the non-dimensional analysis, the following Reynolds numbers were found: flow cell (Re_{fc}), inlet channels (Re_c), gap between posts (Re_g), and flow around an object (Re_o)

where the object is a cylindrical post. This allowed us to quickly and reasonably assess (1) if flow conditions were hydrodynamic and (2) the most probable cause of hydrodynamic conditions. Re_{fc}, Re_c, and Re_g were calculated as follows:

$$Re_{fc} = \frac{2Q}{\nu(h_{fc} + w_{fc})}$$

$$Re_c = \frac{2Q}{n\nu(h_{fc} + w_c)}$$

$$Re_g = \frac{2Q}{n\nu(h_{fc} + w_g)}$$

Where Q is the device volumetric flow rate, h_{fc} is the height of the flow cell, and ν is the kinematic viscosity of the fluid: the respective widths of the flow cell, channel, and gap are w_{fc}, w_c, and w_g and n is the number of gaps or channels and is calculated by:

$$n = \frac{w_{fc}}{p_r}$$

Where p_r is the row pitch. Re_o may be calculated as follows:

$$Re_o = \frac{v_\infty}{\nu}$$

where v_∞ is the free stream velocity and d is the post diameter. v_∞ is calculated as follows:

$$v_\infty = \frac{Q}{h_{fc} w_{fc}}$$

Re_O is then used to calculate the Strouhal number (St) for a smooth cylinder[37] using the following equations:

$$St = 0.21\left(1 - \frac{21}{Re_o}\right) \quad 40 < Re_o < 200$$

$$St = 0.198\left(1 - \frac{19.7}{Re_o}\right) \quad 250 < Re_o < 2\ x\ 10^5$$

St is then used to approximate the frequency (f) of vortex shedding using the following equation:

$$f = \frac{St v_\infty}{d}$$

We also used standard two-dimensional computational fluid dynamics techniques and ANSYS Fluent to simulate hydrodynamic conditions in the unit array geometry using v_∞ as the inlet velocity. This was done to assess *μVS* flow development time at representative hydrodynamic conditions. *μVS* flow development time was simulated by examining the transient drag and lift coefficients acting on the posts while also looking at velocity contours (Figure 1i).

2.3. Pan T cell Culture

Primary CD3+ cells were negatively selected from single donor PBMCs (denoted as pan T cells or T cells) using standard techniques and provided as a gift by Eureka Therapeutics. For revival and culture, 5 x 10^6 cryopreserved pan T cells were expanded using Stemcell Technologies CD3/CD28 T cell activator and standard conditions (details in SI) for 16 days to achieve sufficient cell numbers for the experimental workflow and to allow T cells to return to a resting state based on activation and exhaustion marker expression.

2.4. EGFP mRNA delivery at different concentrations to primary T cells

All solutions used on chip were filtered using 0.22 µm filtration prior to use to remove particulates that could lead to clogging. For on chip cell processing, T cells were removed from culture, washed, and resuspended in processing medium consisting of Immunocult-XF (StemCell Technologies), 25 mM trehalose dihydrate NF (JT Baker, VWR) and 5% v/v DMSO (Corning Cellgro, Fisher Scientific) and filtered using a sterile 40 µm cell filter. Three replicate samples of the eight conditions tested were prepared to have the same final cell concentration of 16 x 10^6 cells mL^{-1} upon mRNA addition and processing of 400 µL cell solution.

The sample rig and tubing were sterilized before use via 70% ethanol wipe down and the tubing cleaned with an ethanol flush. Immediately before processing, each sample was mixed with the appropriate volume of EGFP mRNA (996 nucleotides translated into a 26.9 kDa protein, 1 mg mL^{-1} TriLink BioTechnologies, San Diego CA, L-7601) at final concentrations ranging from 10 µg mL^{-1} to 160 µg mL^{-1} (30 nM to 473 nM). The sample was mixed thoroughly, mounted in the Eppendorf tube fitting, and exposed to 120 psig nitrogen pressure to drive the sample through the chip to induce intracellular mRNA uptake via *μVS* (see Figure 1a-e). Processed sample was collected in a 15 mL conical tube and held on ice until the completion of the experiment, in order to sync expression time points between the different samples, with the maximum time on ice being less than 4 h. After each run, the rig and tubing were flushed with 70% ethanol and a new microfluidic chip was replaced in the rig. Time equals zero for mRNA expression started when all samples were processed, removed from ice and returned to culture medium. Control samples were set up in triplicate and allowed to sit at room temperature while the experimental samples were processed before placement on ice. Control samples that were not device processed consisted of 16 x 10^6 cells mL^{-1} in pure processing medium (handling control) and in processing medium containing 160 µg mL^{-1} mRNA (mRNA control), and were used to normalize the cell viability, mRNA endocytosis (shown to be negligible), and recovery for the experimental samples. Additional device control samples were set up at 16 x 10^6 cells mL^{-1} in pure processing medium and ran through the device to determine the impact of *μVS* on cell survival and state without additional external factors.

2.5. Post processing cell culture, growth, and persistence analysis

After the last sample was processed and iced, count samples were removed for post processing cell viability and concentration quantitation. The remaining samples were diluted in X-VIVO10 at a concentration of around 8 x 10^5 cells mL^{-1} with 100 IU mL^{-1} IL-2 and cultured in 6 well non-TC treated plates at 37 ˚C in 5% CO_2 for growth, viability, activation marker, and EGFP expression analysis at later times. Additional IL-2 was added on days 2 and 4 after transfection and the cells were discarded on day seven after the experiment.

Initial T cell viability and post processing concentration were used to determine the recovery and yield shown in Figure 2a. Cell growth and viability of each sample in growth medium was monitored over a period of seven days using Countess II automated cell counter with trypan blue dye exclusion (Figure 3, blue and black curves). EGFP expression and persistence at different time points post transfection (Figure 3 green curve) was monitored using flow cytometry (Attune NxT flow cytometer) with propidium iodide (1 μM final concentration, Sigma Aldrich) to exclude dead cells.

Expression efficiency along with cell recovery and cell viability were enumerated as a function of mRNA concentration to determine the mRNA concentration that results in the highest yield of recovered, viable and transfected cells where yield is defined as:

$$y = rve$$

where y is yield or the fraction of recovered, viable and transfected cells or percent of input cells that remained viable and expressed EGFP after device transfection. r is the fraction of recovered cells. v is the viability of the recovered cells. e the efficiency of transfection or the fraction of viable cells expressing EGFP.

Yield and efficiency of EGFP expression (Figure 2b) were calculated using the highest EGFP expression value for the cultures, which occurred at approximately 19 hr post processing and return of the cells to culture medium.

2.6. Even Expression Amongst T cell Subtypes

Expression efficiency was examined among CD4+ and CD8+ T cell subtypes using fluorescent monoclonal antibody labeling and flow cytometry analysis 27 h after being returned to culture. Samples were removed from each of the 10, 80, and 160 μg mL^{-1} cultures, rinsed and re-suspended in 100 μL of 25 μL mL^{-1} each fluorescently labeled mouse anti-human CD3, CD4, and CD8 in DPBS containing 1% bovine serum albumin and 2 mM EDTA (FACS buffer) to quantify the percentage of CD4+ and CD8+ T cell subtypes expressing EGFP. Labeled cells were analyzed via flow cytometry and compensated using a combination of AbC compensation beads (ThermoFisher) labeled with the above antibodies and EGFP expressing cells (BL1 channel, details in SI).

2.7. No Change in T cell Activation

To assess the impact of *μVS*-based mRNA delivery on T cell activation, one sample per activation marker from each replicate in the control and device processed (no mRNA) groups were labeled with fluorescent labeled antibodies against various activation markers 24 h after return to culture. Samples were rinsed and re-suspended in FACS buffer containing 25 μL mL^{-1} of one of the following ThermoFisher monoclonal anti-human antibodies per sample (details in SI): CD40L/CD154, CD25, CCR7, CD44, CD69, and CD45RA. The samples were incubated on ice for 30 minutes, rinsed, and analyzed via flow cytometry.

3. Results & Discussion

3.1. Hydrodynamic Characterization

Non-dimensional analysis was used to characterize flow conditions in the (1) device flow cell, (2) inlet channels, (3) between posts, and (4) around the posts. Hydrodynamic conditions were characterized and simulated using a kinematic viscosity of 1.004×10^{-6} m^2 s^{-1} or that of water at 20 ˚C, as cell medium consists mostly of water, and transfections were done at room temperature (approximately 20 ˚C). Different transfection media compositions were shown to have similar dynamic viscosity to water at 20 ˚C at high shear rates (not shown). Moreover, the purposes of the hydrodynamic characterization and simulation is to provide a reasonable analysis of the hydrodynamic conditions. To this end, a summary of the non-dimensional analyses is shown in Table 1 below:

Table 1 Non-dimensional and hydrodynamic characterization of *μVS*

Feature	Units	Value
Flow cell Reynold's number (Re_{fc})	—	271
Channel Reynold's number (Re_c)	—	180
Gap Reynold's number (Re_g)	—	291
Object Reynold's number (Re_o)	—	146
Strouhal number (St)	—	0.18
Frequency (f)	kHz	14.8

The table above shows that flow conditions within the flow cell (Re_{fc}), channels (Re_c) and at the gap between posts (Re_g) are 271, 180, and 291 respectively. These values are well below the Reynolds number for the onset of transitional and turbulent flow[37]. Thus, flow conditions upstream of the post array are laminar and the hydrodynamic conditions within the microfluidic device can be attributed solely to vortex shedding since $Re_o = 146$ and vortex shedding is known to occur when $Re_o > 40$[37].

Microfluidic fluid dynamics are well studied with Reynolds number-matched micro- and macro-scale flows having the same characteristics in complex flow conditions[38]. Furthermore, vortex shedding has been previously shown to occur in microfluidic post arrays[39]. Vortex shedding occurs in the near wake behind posts, and due to the flow instability, resulting in fluctuating flow fields and thus drag and lift forces. Thus, it is reasonable to conclude vortex shedding is occurring in these specific microfluidic post arrays.

Simulation via computational fluid dynamics was also used to confirm the hydrodynamic flow conditions, showing the development of vortices in the wake and it was thereby possible to investigate the vortex shedding frequency, and determine flow development times for *μVS*. Flow development time was used to assess what percentage or fraction of each sample is exposed to fully-developed *μVS* and to approximate the minimal theoretical sample size. As shown in Figure 1i, flow conditions are fully-developed after approximately 10^{-4} s. Furthermore, drag coefficient analyses suggests *μVS* flow development time is 3 x 10^{-4} s at a device flow rate of 8 mL min^{-1} or the typical initial flow rate observed during this study.

Flow development times therefore account for an estimated 0.01% of total sample flow time when 400 μL samples are processed. This is particularly significant when small samples are needed for research applications where minimal reagent consumption is ideal. At even smaller volumes *μVS* development times still represent a minute fraction of total flow times – a 40 μL sample, for example, would have fully-developed *μVS* conditions for 99.9% of the sample during processing. In this flow condition, vortex-shedding occur behind cylinders affected each other and near anti-phase synchronized regime is dominate flow pattern.

3.2. *μVS* design analysis

The on chip hydrodynamic characterization and simulation methods in the previous section assumed single-phase fluid dynamics, which is viewed as reasonable given the focus of this manuscript. The region immediately between the fabricated posts contains a volume of approximately 4.6 pL whereas each individual cell occupies a suspension volume of approximately 62.5 pL at a cell concentration of 16 x 10^6 cells mL^{-1} – suspension volume refers to the total volume of a single cell and surrounding suspension medium assuming even distribution of suspended cells in the medium. This means the total suspension volume per cell is 13.6-fold greater than the volume immediately between posts. It was assumed cells are individually processed with negligible cell-cell interaction when passing through the post array and single-phase fluid dynamics is a reasonable assumption when characterizing and simulating the flow conditions. Furthermore, pan T cells from this donor are typically 8 to 10 μm in diameter. A 9 μm diameter sphere has a volume of 0.38 pL – a typical pan T cell from this donor occupies a volume that is 12.1-fold smaller than the volume immediately between posts. Cell-post interaction is minimal for cells positioned near the middle of each channel. Channel widths and heights are approximately 6.6-fold and 4.4-fold greater than typical pan T cell from this donor suggesting most cells flow immediately between the posts. These relative volumes and geometries mean the major interactions are fluid-cell or fluid-post interactions such that more advanced three-dimensional and multi-phase simulations were not necessary. In previous post array optimization simulations and studies, it was observed that post spacing directly impacts transfection efficiency, with cell types with smaller diameters needing closer post spacing, where the ideal spacing is approximately two-fold greater than average cell diameter within a specific cell population.

Further studies in to the accurate tracking of suspended cells trajectories would require high speed microscopy capabilities capable of capturing images of cells traveling at estimated velocities of approximate 10 to 15 m s^{-1}. Imaging at different focal planes may also allow for assessing interactions or lack thereof between the top and bottom of the channel. A meaningful amount of studies have been published with regard to cell and particle trajectories in microfluidic channels[40],

however, *μVS*-specific high-speed microscopy studies may be required to accurately assess the impact of *μVS*-specific fluid dynamics on suspended cell trajectories. Fundamental research into *μVS*-specific fluid dynamics using micro-particle image velocimetry (*μPIV*) and contact vibrometry (the techniques used by Renfer *et al.*)[39] are not warranted and unlikely to yield accurate results given the particle suspensions used for *μPIV* are likely to have undesirable biological implications (e.g., cytotoxicity) and contact vibrometry perturbs the system being measured. Given the accuracy considerations described above, any fundamental research in to *μVS*-specific multi-phase fluid dynamics should focus on high speed optical microscopy coupled with non-contact laser vibrometry techniques. This would provide the most accurate data on (1) suspended cell trajectories analysis along with (2) hydrodynamic conditions.

Additional fundamental research into the impact of array size, channel depth, post diameter, post shape, transversal pitch, longitudinal pitch along with pitch orientation may be warranted. In preliminary experiments, both a post diameter and post gap of approximately two-fold the average cell diameter seemed to be the optimal configuration. In preliminary experiments, an array length of 5 to 7 posts resulted in optimal yield. Different cross-sectional post shapes (e.g., circular, triangular and rhomboid) with the same width did not significantly alter delivery efficiency, cell viability nor cell recovery. Further research into the influence of channel depth may prove useful when developing both lower- and higher-throughput designs. For higher-throughput design, however, channel depth will be limited by the aspect ratio or ratio of height to width of the channel wall. The design described in this manuscript utilizes a fabricated aspect ratio of 6.6.

In this experiment, initial flow rates between 6 to 10 mL min^{-1} were observed for each sample, as measured using a volumetric flow meter. The flowrate decays over time to 4 to 6 mL min^{-1} and to a larger degree with larger volume samples than those used in herein. In the future, we are working to reduce cell debris buildup through (1) flow path optimization, (2) device design, (3) using addition of surfactants and (4) investigating the effect ionic strength on cell buildup, as it was observed that higher mRNA concentration samples had higher amounts of buildup compared to lower mRNA concentration samples.

As build up does occur due to mechanical lysis towards the end of the processing, it was necessary to evaluate if this buildup was resulting in cell constriction-based deformation and poration. If cell constriction was the cause of transfection, it would require buildup of lysed cell debris. As buildup requires time to form, samples collected at the end of the run would have significantly higher transfection efficiency than samples collected earlier in the sample processing, as there is no initial channel constriction due to post build up at early times. Samples collected from initial processing time points (e.g., first ~100 μL of cells processed) would also show little or no transfection efficiency while the last 100 μL of sample would show the highest transfection efficiency.

To assess this, we processed cells using the same concentration screen (different donor, 80 μg mL^{-1} mRNA) and collected the processed cells in dropwise fractions as they were eluted off the chip. Fractions of 1-3 drops per well were collected in wells of a 96 well plate and were analyzed individually for transfection efficiency vs. time processed on chip. Each fraction collected showed similar transfection efficiency of an average 32.7% ± 5.6% percent EGFP+ cells throughout the fractions (data not shown). The transfection efficiency was observed to increase slightly with increasing faction number, but not to the degree expected if cell constriction was the main method

of cell poration and transfection. Additionally, no EGFP+ cells would be present in initial fractions if poration was based solely due to constriction. Thus, cell build up throughout the experiment processing time caused negligible impact on transfection efficiency, with poration being attributed to *μVS*.

3.3. EGFP mRNA delivery at different concentrations to primary T cells using *μVS*

High efficiency and low time requirement transfection methods like electroporation often result in reduction of cell viability and recovery in T cells[11,12,41]. Comparatively, *μVS*-based molecule delivery substantially reduces processing time and impact on T cell health. Delivery of 30 to 473 nM EGFP mRNA to pan CD3+ cells resulted in maximum EGFP expression ranging from approximately 20% to 65% of the live, processed cell population at 19 h (Figure 2a-b). Interestingly, the median live cell population EGFP fluorescence intensity is linearly correlated with mRNA concentration (Figure 2c). The median intensity error is higher in this plot for mRNA concentrations > 40 μg mL^{-1} due to the larger distribution of fluorescence intensity (between 0 and greater than 1 x 10^6 relative fluorescence units) compared to lower concentration samples, where max fluorescence is less than 1 x 10^6 RFU. Short processing time (e.g., approximately 3 s for 400 μL samples) allows for cells to be returned to cell culture medium immediately after processing. This promotes rapid recovery and reduces stress and damage that occurs to cells from long periods of time in low or serum free medium, such as the conditions required for chemical transfection. Additionally, *μVS* is a seemingly gentler intracellular delivery method when compared to electroporation, resulting in high recovery (e.g., greater than 88%) and viability (e.g., greater than 77%) in all conditions tested, whereas electroporation can result in low viability and recovery, especially for primary immune cells.

We found that medium composition has a direct impact on cell recovery and viability as well as overall efficiency for *μVS* mRNA delivery. We screened a variety of serum free media and found that overall yield (*y*) was highest for Immunocult-XF compared to other serum free medium options, including the X-VIVO10 medium used to propagate the T cells. Trehalose was added to the medium as it was shown to enhance cell viability and recovery during medium screening (data not shown) and has been demonstrated to reduce cell loss during electroporation[42]. Finally, 5% v/v dimethyl sulfoxide (DMSO) was added to the processing medium as a cosolvent, using short cell exposure times, with the idea of increasing the ease of pore generation or perhaps size of the pore in the cell membrane upon exposure to *μVS*. 24 hr incubation in low concentrations of DMSO has been shown to increase cationic lipid chemical transfection efficiency with human embryonic stem cells[43], and to generate pores in mammalian cells for intracellular DNA delivery with polybrene[44]. In these examples, addition of a DMSO is thought to aid in the reduction of membrane resistance to poration, further supporting its use to enhance membrane pore formation with *μVS*.

The impact of exposure of human primary blood mononuclear cells (PBMCs) to DMSO for long periods of time in culture conditions (37 ˚C, 5% CO_2), was reported by de Abreu Costa *et al.* In this study, long term exposure to various concentrations of DMSO resulted in increased cell death, decreased proliferation, and reduced cytokine production with increasing DMSO concentrations and long exposure times (>4 h), after activation with phorbol-12-myristate-13-acetate (PMA).[45] This study showed that DMSO at 5% v/v did not impact cell viability until PBMCs were incubated in this solution for greater than 24 h exposure times at 37 ˚C and 5% CO_2 (24 h and 120 h time points were explored). Cytokine production by PMA activated T cells was negatively impacted by

exposure to 5% DMSO, but required eight hours of incubation time, four hours after being activated. The max time for samples in processing medium was under four hours, and the samples were held on ice, not 37˚C. The cells were processed in the order of lowest to highest mRNA concentration meaning 10 µg mL^{-1} spent the longest time on ice exposed to DMSO post processing. This could be why the growth rate of this group cells was reduced post processing compared to the other groups, meaning that this reduction in growth rate is an artifact due to the experiment length. Additionally, the decrease in viability and relatively lower growth rate of the 10 µg mL^{-1} sample (see Figure 3c) compared to the other concentration is hypothesized to be a result of extended time on ice in processing medium (3.5 to 3.75 h total for these samples). The decrease in viability of all groups compared to the handling control may be due to increased cell death upon return to culture due to unsuccessful membrane repair attempts, bulk mechanical lysis along with thermal shock, and medium stress, but this viability decrease is small when considering the device processed control.

Processing medium ionic strength may also have an impact on the overall ease of pore formation and cell recovery after *µVS* exposure. We observed a trend of decreasing viability with increasing mRNA concentrations, though this decrease was slight. This was potentially due to the higher percentage of mRNA solution added to samples containing higher concentrations of mRNA. For example, a 10 µg mL^{-1} sample contained 1% v/v mRNA buffer in the processing medium, while 160 µg mL^{-1} sample contained 16% v/v mRNA buffer. The mRNA solution is at a low ionic strength buffer (1 mM sodium citrate) relative to Immunocult-XF. This means that the reduction in total processing medium ionic strength associated with increasing mRNA concentration is likely the cause of decreasing viability trend. The presence of the mRNA solution also decreases the concentration of trehalose, which could also result in lower cell viability with increasing mRNA concentration. In the future, this variable will be further explored and addition of concentrated buffer mixes will be used to adjust final ionic strength.

The total cell recovery rates for *µVS* were exceptionally high. Zhang *et al.* reported T cell recovery rates of 20% after electroporation[12], meaning *µVS* offers a nearly 5-fold improved T cell recovery relative to this. Along with low recovery, electroporation is also known to adversely affect T cell viability. Bilal *et al.* reported T cell viability ranging from 15% to 40% after electroporation[41]. They also observed further cell death over 2 to 3 days particularly when high concentrations of plasmid were used. *µVS*, on the other hand, does not affect cell viability nor cell growth relatively to handling and mRNA controls (Figure 3). A slight decrease in T cell viability and growth is observed when comparing the mRNA control (Figure 3b) to the 160 µg mL^{-1} (Figure 3g), however, it is small. When comparing the device processed control cells (Figure 3h) to the handling control (Figure 3a), the growth rate and viability are nearly identical over the entire seven day culture period, indicating that the modest reduction in viability and growth rate for mRNA processed cells is likely due to the presence of the mRNA solution and not the effects of processing cells using *µVS*. Cumulatively, this suggests *µVS* is a gentler method for T cell intracellular delivery relative to electroporation, allowing for significant yield of recovered, viable, and EGFP expressing T cells.

3.4. Even Expression Profiles in T cell Subtypes

To assess if there was a population bias for *µVS* mRNA delivery, samples of T cells from three different mRNA concentrations were labeled with anti-CD3, CD4, and CD8a fluorescent

antibodies and the distribution of T cell types EGFP fluorescence was analyzed via flow cytometry. The results shown in Figure 4 demonstrate equal percentages of EGFP expressing cells in CD4+ and CD8+ populations throughout all experimental conditions (10, 80, and 160 μg mL^{-1}). Additionally, the mRNA concentration-dependent fluorescent intensity profiles are also nearly identical showing reproducibility between the CD4+ and CD8+ T cell subtypes.

This equal distribution is advantageous for GMCTs focused on using mixtures of CD4+ and CD8+ T cells instead of isolating a pure population of T cells. It is also advantageous for point-of care GMCT manufacturing where less pre-processing of PBMCs prior to genetic manipulation and re-infusion is preferred. These even distribution profiles may also be unique to *μVS*. Lentiviral transduction efficiencies are known to differ amongst T cell subtypes without a consistent trend between donors[46] while electroporation is shown to adversely affect CD8+ T cell populations resulting in 40% CD8+ T cell viability[13]. Furthermore, expression profiles are known to differ between CD4+ and CD8+ T cells after plasmid electroporation[28]. Cumulatively, the data shown in Figure 4 demonstrate even expression profiles amongst CD4+ and CD8+ T cell subtypes after cytosolic delivery of EGFP mRNA and suggest that *μVS* may provide an additional advantage over electroporation and lentiviral transduction at least when considering cytosolic intracellular delivery. Further investigation into the expression profiles with alternative constructs such as plasmids and Cas9 RNPs across multiple donors is ongoing.

3.5. No Change in T Cell Activation

It has been observed that electroporation of primary human immune cells increases activation markers in T cells. 24 hours after electroporation and return to culture, Zhang and Ma *et al.* observed an increase in expression of CD69, an early marker of T cell activation, and CD154, an activation marker that serves in co-stimulation of antigen presenting cells, indicating that electroporation results in activation of CD4+ T cells[12]. For this reason, we examined whether processing cells using *μVS* would result in a change in the cell activation state compared to cells in culture (see Figure 5). Each replicate from the handling control, and device processed control groups were individually labeled with different antibodies against activation markers CD69 and CD154, as well as the additional markers of activation CCR7, CD25, CD45RA, and CD44. CCR7 is a lymphoid homing cytokine receptor found on naïve T cells and is lost upon activation. CD25 is a later marker of activation compared to CD69, which increases upon cell activation and persists on activated the cell surface longer than CD69. CD45RA is found on naïve T cells and is lost upon activation and formation of memory. CD44 is a receptor for specific extracellular matrix components and is upregulated upon T cell activation. When analyzed 24 h after processing, a shift in the histogram shape, population distribution, or change in fluorescence intensity for the device processed cells compared to that of the handling control would demonstrate that *μVS* exposure impacts T cell activation state. Isotype control for mouse IgG1 kappa was previously determined to have no off target or non-specific binding interactions with the T cells used in this experiment (not shown). Thus, shifts in fluorescence intensity for the various markers would be due to specific interactions.

Device processed cells and control cells show similar expression for all markers (Figure 5 shows representative data from a replicate from each group). Histogram data from both groups mapped almost identically, indicating that *μVS* does not alter the activation state of T cells 24 h after

processing. This is advantageous as intracellular delivery with *μVS* results in high viability and recovery but does not perturb the state of T cell activation, an important attribute in CAR-T therapies, in contradistinction to results seen using electroporation.

3.6. Clinical- and commercial- considerations with *μVS* microfluidic device.

A reduction in delivery efficiency was observed when post spacing is increased to greater than that of the cell diameter, however, this is compensated for by exceptionally increased processing rate and cell recovery. The tradeoff for reduced efficiency is increased flow rate, sample size, and cell concentration tolerance, while eliminating clogging observed with other microscale methods that rely on cell constriction. Also, the very short time spent in poration conditions during *μVS* results in a gentler transfection method, which in turn limits cell stress. Further studies are planned to examine calcium release immediately after processing to verify this. Together, these characteristics of *μVS* transfection positions it as the only current microscale transfection method suitable for generation of clinically-relevant scales of cells for GMCT for a wide range of therapies ranging from cancer to diabetes.

Non-viral RNA delivery is an attractive approach for GMCT generation to circumvent use of infectious viral particles, which require more clinician hands on time along, long-term safety monitoring, and release testing.[2,29,47] Additionally, the long lead times for therapeutic virus (up to 24 months) means GMCT gravely needs an alternative solution to viral vectors to address the growing number of patients in need of GMCT.

Specifically, CAR-T therapy is severely dependent upon viral vector supply and would greatly benefit from alternate methods of therapy generation. *μVS* is a promising solution to this problem and has additional benefits of greatly reducing manufacture time, safety concerns, and release testing requirements. For example, the maximum dosage for the first two FDA approved CAR-T therapies, Yescarta and Kymriah, is 200 x 10^6 and 250 x 10^6 CAR^+ T cells per patient, respectively, delivered in a single infusion. Expansion modelling indicates more than the maximum allowable dose can be produced using the *μVS* device design described in this study.

To achieve this, we have explored processing samples with cell concentrations up to 100 x 10^6 T cells mL^{-1} using our platform, and in its current state, it can process concentrations of 50 x 10^6 cells mL^{-1} without clogging while maintaining high flow rates. 45% yield was observed in this study and processing 1 mL of 50 x 10^6 cells to deliver CAR RNA, we can achieve approximately 23 x 10^6 CAR^+ T cells in less than 1 minute. Upon expansion of these cells using the CAR antigen, 4 doubling times (2 ~ 4 days post activation) would achieve approximately 360 x 10^6 CAR-T cells or substantially more than maximum allotted dose for Yescarta and Kymriah. This means that *μVS*-based GMCT manufacturing would require under 5 days between cell harvesting and finalized therapy manufacture, not including release testing. In practice, sequential sterility testing may increase total manufacturing time to between 9 and 11 days when using *μVS*. However, improvements in net yield and throughput would further reduce expansion time requirements.

Additionally, larger scale ElveFlow tube adaptors that can accommodate 15 and 50 mL conical tubes would allow for more convenient large-scale therapy generation. By processing 10 mL of cells at the above concentration, *μVS* transfection would generate up to the maximum therapeutic dose of CAR^+ T cells required by both Yescarta and Kymriah in under 10 minutes. The cost of

reagent required for 10 mL processing may prove prohibitive for autologous GMCTs, however, it may be more viable for allogeneic GMCTs, where numerous doses are expanded out from an initial sample. On the other hand, this immediate turn around could be reinfused immediately, making the time from apheresis to treatment less than one day if *μVS* were to be engineered into a completely closed system to avoid release testing requirements. We have observed cell type, age, time post activation and medium composition all impact debris accumulation rate. In the future we plan to further optimize these parameters in conjunction with exploration addition of detergents and channel coating as ways to increase cell concentrations for processing to 100 x 10^6 cells mL^{-1}. Achieving concentrations above this will greatly reduce the turnaround times for clinically- and commercially-relevant GMCT generation while further supporting the use of *μVS* as the optimal method for GMCT manufacture.

4. Conclusions & Future Work

The work presented herein described the use of microfluidic post array used to create hydrodynamic conditions based on vortex shedding, or *μVS,* enabling the intracellular delivery of mRNA to human pan T cells. This method and device enabled the efficient delivery of mRNA to T cells with high cell recovery (e.g., 96.3 ± 1.1%, mean ± stdev), high cell viability (e.g., 83.7 ± 0.7%) and meaningful EGFP expression (e.g., 57.4 ± 6.8%) resulting in a yield of 46.3 ± 5.6% recovered, viable, and EGFP expressing pan T cells when delivering mRNA at a concentration of 80 μg mL^{-1} and at a processing rate of greater than 2 x 10^6 cells s^{-1}. *μVS* is also shown to result in even EGFP expression profiles within CD4+ and CD8+ T cell populations without changing T cell activation state. Conveniently, the microfluidic devices are fabricated with industry standard processes and relatively simple feature geometries allow for (1) high device yields that are thought to (2) readily scale.

The focus of future work will be three-fold: (1) advanced T cell modification through functional mRNA constructs encoding for the Cas9 protein and gRNA, or chimeric antigen receptors along with (2) modification of alternative cell types isolated or enriched from peripheral blood using different constructs (e.g., plasmids and Cas9 ribonucleoprotein complexes) and (3) verification of the resultant *μVS* protocols in multi-donor studies for healthy and disease patient samples. Additional separation and enrichment steps prior to *μVS* delivery may be required for disease patient samples.

Future work could also involve adapting *μVS* to different cell types such as those in the myeloid lineage, which may require cell-type specific design, media and operating pressure optimization particularly if using disparate cell types.

Acknowledgments

The authors would also like to thank Simon Doe, Hamish Hawthorn, Ben Wright, Mike Nicholls, Warren McKenzie, Todd Martin, Niranjana Nagarajan, Steve Gourlay, Mike Bowles, Geoff Facer, and Heidi Hagen for the guidance, advice and assistance when it comes to pursuing science in the startup environment. This work was funded in part by IndieBio (indiebio.co), SOSV (sosv.com), Jobs for NSW (jobsfornsw.com.au), Y Combinator (ycombinator.com), AusIndustry, Social+Capital, Main Sequence Venture and Founders Fund along with an array of angel investors.

The microfabrication work was performed in part at the South Australia node of the Australian National Fabrication Facility, a company established under the National Collaborative Research Infrastructure Strategy to provide nano- and micro-fabrication facilities for Australia's researchers. Single donor human primary T-cells were provided as a gift by Eureka Therapeutics, Inc. The content is solely the responsibility of the authors and does not necessarily represent the views of anyone acknowledged in this section.

Conflicts of Interest

All authors are consultants, employees, shareholders and/or optionees of Indee. Inc. and/or the wholly-owned Australian subsidiary Indee. Pty. Ltd. Both entities have an interest in commercializing *μVS* and related technologies.

References

1. Shields, C. W., Reyes, C. D. & López, G. P. Microfluidic cell sorting: a review of the advances in the separation of cells from debulking to rare cell isolation. *Lab. Chip* **15,** 1230–1249 (2015).
2. Stewart, M. P. *et al. In vitro* and *ex vivo* strategies for intracellular delivery. *Nature* **538,** 183–192 (2016).
3. Mehling, M. & Tay, S. Microfluidic cell culture. *Curr. Opin. Biotechnol.* **25,** 95–102 (2014).
4. Zilionis, R. *et al.* Single-cell barcoding and sequencing using droplet microfluidics. *Nat. Protoc.* **12,** 44–73 (2017).
5. Kochenderfer, J. N. *et al.* Long-Duration Complete Remissions of Diffuse Large B Cell Lymphoma after Anti-CD19 Chimeric Antigen Receptor T Cell Therapy. *Mol. Ther. J. Am. Soc. Gene Ther.* **25,** 2245–2253 (2017).
6. Ledford, H. Engineered cell therapy for cancer gets thumbs up from FDA advisers. *Nat. News* **547,** 270 (2017).
7. Wang, X. & Rivière, I. Clinical manufacturing of CAR T cells: foundation of a promising therapy. *Mol. Ther. Oncolytics* **3,** 16015 (2016).
8. Vormittag, P., Gunn, R., Ghorashian, S. & Veraitch, F. S. A guide to manufacturing CAR T cell therapies. *Curr. Opin. Biotechnol.* **53,** 164–181 (2018).
9. Tchou, J. *et al.* Safety and Efficacy of Intratumoral Injections of Chimeric Antigen Receptor (CAR) T Cells in Metastatic Breast Cancer. *Cancer Immunol. Res.* **5,** 1152–1161 (2017).
10. Levine, B. L., Miskin, J., Wonnacott, K. & Keir, C. Global Manufacturing of CAR T Cell Therapy. *Mol. Ther. - Methods Clin. Dev.* **4,** 92–101 (2017).
11. Ramanayake, S. *et al.* Low-cost generation of Good Manufacturing Practice-grade CD19-specific chimeric antigen receptor-expressing T cells using piggyBac gene transfer and patient-derived materials. *Cytotherapy* **17,** 1251–1267 (2015).
12. Zhang, M. *et al.* The impact of Nucleofection® on the activation state of primary human CD4 T cells. *J. Immunol. Methods* **408,** 123–131 (2014).
13. Liu, L., Johnson, C., Fujimura, S., Teque, F. & Levy, J. A. Transfection optimization for primary human CD8+ cells. *J. Immunol. Methods* **372,** 22–29 (2011).
14. Hallow, D. M. *et al.* Shear-induced intracellular loading of cells with molecules by controlled microfluidics. *Biotechnol. Bioeng.* **99,** 846–854 (2008).

15. Bürgel, S. C., Escobedo, C., Haandbæk, N. & Hierlemann, A. On-chip electroporation and impedance spectroscopy of single-cells. *Sens. Actuators B Chem.* **210,** 82–90 (2015).
16. Huang, Y. & Rubinsky, B. Flow-through micro-electroporation chip for high efficiency single-cell genetic manipulation. *Sens. Actuators Phys.* **104,** 205–212 (2003).
17. Zu, Y., Huang, S., Lu, Y., Liu, X. & Wang, S. Size Specific Transfection to Mammalian Cells by Micropillar Array Electroporation. *Sci. Rep.* **6,** 38661 (2016).
18. Chow, Y. T. *et al.* Single Cell Transfection through Precise Microinjection with Quantitatively Controlled Injection Volumes. *Sci. Rep.* **6,** 24127 (2016).
19. Sharei, A. *et al.* A vector-free microfluidic platform for intracellular delivery. *Proc. Natl. Acad. Sci. U. S. A.* **110,** 2082–2087 (2013).
20. Li, J. *et al.* Microfluidic-Enabled Intracellular Delivery of Membrane Impermeable Inhibitors to Study Target Engagement in Human Primary Cells. *ACS Chem. Biol.* **12,** 2970–2974 (2017).
21. Han, X. *et al.* CRISPR-Cas9 delivery to hard-to-transfect cells via membrane deformation. *Sci. Adv.* **1,** (2015).
22. Sharei, A. *et al.* Ex vivo cytosolic delivery of functional macromolecules to immune cells. *PloS One* **10,** e0118803 (2015).
23. Sharei, A. *et al.* Cell Squeezing as a Robust, Microfluidic Intracellular Delivery Platform. *J. Vis. Exp. JoVE* (2013). doi:10.3791/50980
24. Ding, X. *et al.* High-throughput Nuclear Delivery and Rapid Expression of DNA via Mechanical and Electrical Cell-Membrane Disruption. *Nat. Biomed. Eng.* **1,** (2017).
25. Cencen, V. A Microfluidic Device for Transfection of Mammalian Cells Using Adjustable Shear Stress. (Université d'Ottawa / University of Ottawa, 2016). doi:http://dx.doi.org/10.20381/ruor-483
26. Zarnitsyn, V. G. *et al.* Electrosonic ejector microarray for drug and gene delivery. *Biomed. Microdevices* **10,** 299–308 (2008).
27. Wang, J. *et al.* Highly efficient homology-driven genome editing in human T cells by combining zinc-finger nuclease mRNA and AAV6 donor delivery. *Nucleic Acids Res.* **44,** e30 (2016).
28. Kebriaei, P. *et al.* Phase I trials using Sleeping Beauty to generate CD19-specific CAR T cells. *J. Clin. Invest.* **126,** 3363–3376 (2016).
29. Beatty, G. L. *et al.* Mesothelin-specific Chimeric Antigen Receptor mRNA-Engineered T cells Induce Anti-Tumor Activity in Solid Malignancies. *Cancer Immunol. Res.* **2,** 112–120 (2014).
30. Sahin, U., Karikó, K. & Türeci, Ö. mRNA-based therapeutics--developing a new class of drugs. *Nat. Rev. Drug Discov.* **13,** 759–780 (2014).
31. Rupp, L. J. *et al.* CRISPR/Cas9-mediated PD-1 disruption enhances anti-tumor efficacy of human chimeric antigen receptor T cells. *Sci. Rep.* **7,** 737 (2017).
32. Lundstrom, K. Self-replicating RNA viral vectors in vaccine development and gene therapy. *Future Virol.* **11,** 345–356 (2016).
33. Peng, Y. *et al.* Innate and adaptive immune response to apoptotic cells. *J. Autoimmun.* **29,** 303–309 (2007).
34. Morgenstern, D. A. *et al.* Post-thaw viability of cryopreserved peripheral blood stem cells (PBSC) does not guarantee functional activity: important implications for quality assurance of stem cell transplant programmes. *Br. J. Haematol.* **174,** 942–951 (2016).

35. Watts, M. J. & Linch, D. C. Optimisation and quality control of cell processing for autologous stem cell transplantation. *Br. J. Haematol.* **175,** 771–783 (2016).
36. Woodruff, K. & Maerkl, S. J. A High-Throughput Microfluidic Platform for Mammalian Cell Transfection and Culturing. *Sci. Rep.* **6,** 23937 (2016).
37. Gerhart, P. M., Gerhart, A. L. & Hochstein, J. I. *Munson, Young and Okiishi's Fundamentals of Fluid Mechanics, 8th Edition*. (Wiley Global Education, 2016).
38. Sinclair, A. Steady and oscillatory flow in the entrance region of microchannels. (Awarded By: University of New South Wales Mechanical & Manufacturing Engineering, 2012).
39. Renfer, A. *et al.* Vortex shedding from confined micropin arrays. *Microfluid. Nanofluidics* **2,** 231–242 (2013).
40. Adeyiga, O., Mach, A. J., Rao, J. & Carlo, D. D. Current Status of Microfluidics-Assisted Cytology: The Application in Molecular Cytology. in *Molecular Cytopathology* 261–283 (Springer, Cham, 2016). doi:10.1007/978-3-319-30741-1_15
41. Bilal, M. Y., Vacaflores, A. & Houtman, J. C. Optimization of methods for the genetic modification of human T cells. *Immunol. Cell Biol.* **93,** 896–908 (2015).
42. Mussauer, H., Sukhorukov, V. L. & Zimmermann, U. Trehalose improves survival of electrotransfected mammalian cells. *Cytometry* **45,** 161–169 (2001).
43. Villa-Diaz, L. G., Garcia-Perez, J. L. & Krebsbach, P. H. Enhanced transfection efficiency of human embryonic stem cells by the incorporation of DNA liposomes in extracellular matrix. *Stem Cells Dev.* **19,** 1949–1957 (2010).
44. Aubin, R. A., Weinfeld, M., Mirzayans, R. & Paterson, M. C. Polybrene/DMSO-assisted gene transfer. Generating stable transfectants with nanogram amounts of DNA. *Mol. Biotechnol.* **1,** 29–48 (1994).
45. de Abreu Costa, L. *et al.* Dimethyl Sulfoxide (DMSO) Decreases Cell Proliferation and TNF-α, IFN-γ, and IL-2 Cytokines Production in Cultures of Peripheral Blood Lymphocytes. *Mol. Basel Switz.* **22,** (2017).
46. Turtle, C. J. *et al.* CD19 CAR-T cells of defined CD4+:CD8+ composition in adult B cell ALL patients. *J. Clin. Invest.* **126,** 2123–2138 (2016).
47. Schott, J. W., Morgan, M., Galla, M. & Schambach, A. Viral and Synthetic RNA Vector Technologies and Applications. *Mol. Ther.* **24,** 1513–1527 (2016).

Figures

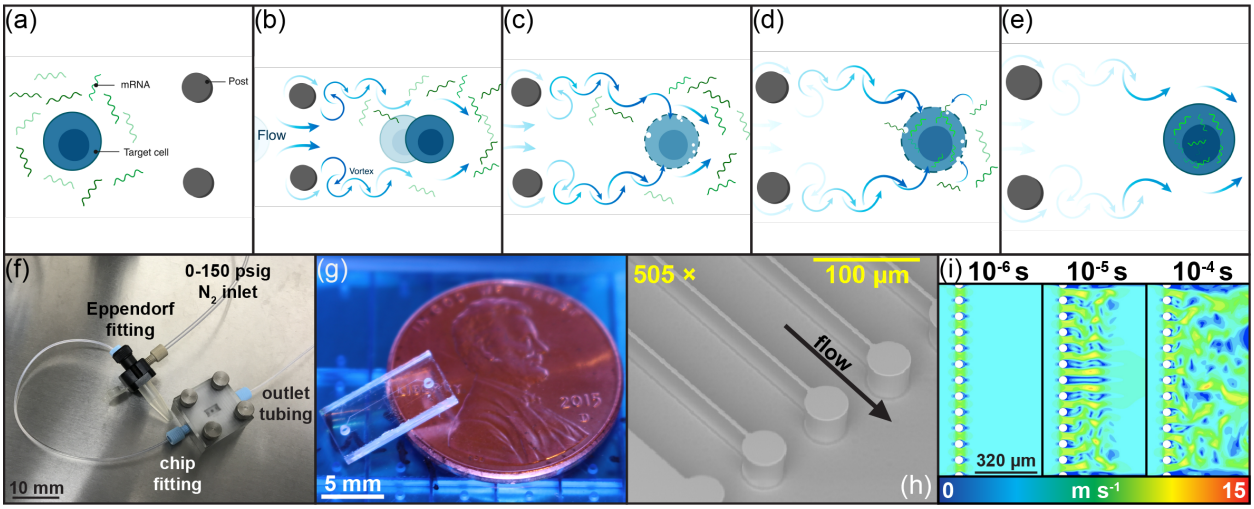

Figure 1 – Overview of *µVS* where (a) cell and mRNA are mixed in suspension, (b) flow of the suspension past posts creates vortices, (c) vortices disrupt the cell membrane, (d) allowing for mRNA to diffuse into the cytosol prior to (e) the cell membrane repairing itself. The hardware unit (f) is used to pneumatically drive the mRNA and cell suspension through the microfluidic chip (g) where the deep reactive ion etched posts (h) create hydrodynamic flow conditions as (i) simulated using computational fluid dynamics. Figures 1a-e are for illustrative purposes only and not drawn to scale.

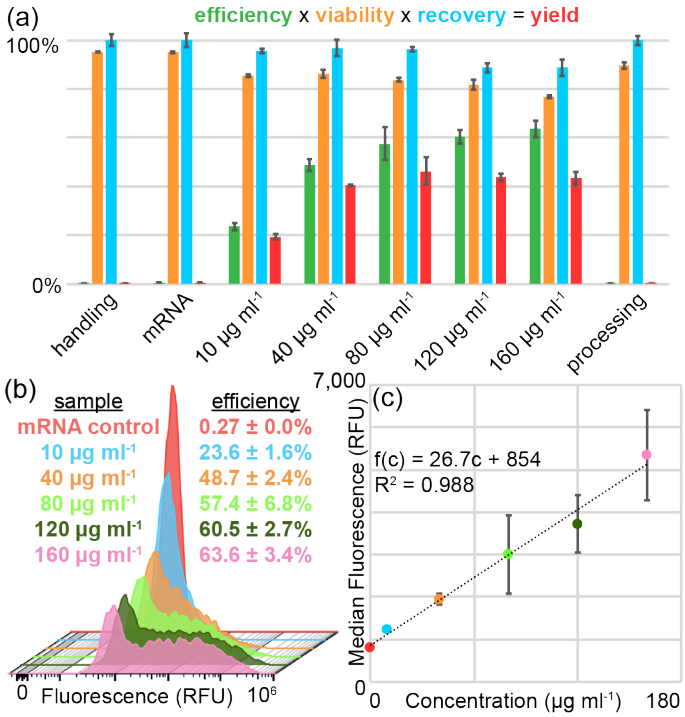

Figure 2 –T cell EGFP expression details. (a) Primary T cell EGFP expression efficiency at 19 h post transfection (green bar), post processing cell viability (orange bar), cell recovery (blue bar), and total yield of transfected cells (red bar) using different mRNA transfection concentrations (n = 3). In all conditions, high recovery (e.g., greater than 88%) and viability (e.g., greater than 77%) was achieved after *µVS* transfection. (b) EGFP expression histograms from live single T cells analyzed via flow cytometry as a function of mRNA concentration at 19 h after transfection and return to culture. Transfection efficiency ranged from approximately 24% to 64% for 10 µg mL^{-1} (30 nM) to 160 µg mL^{-1} (473 nM). (c) There was also a linear relationship between median population EGFP fluorescence (in relative fluorescence units) and mRNA concentration.

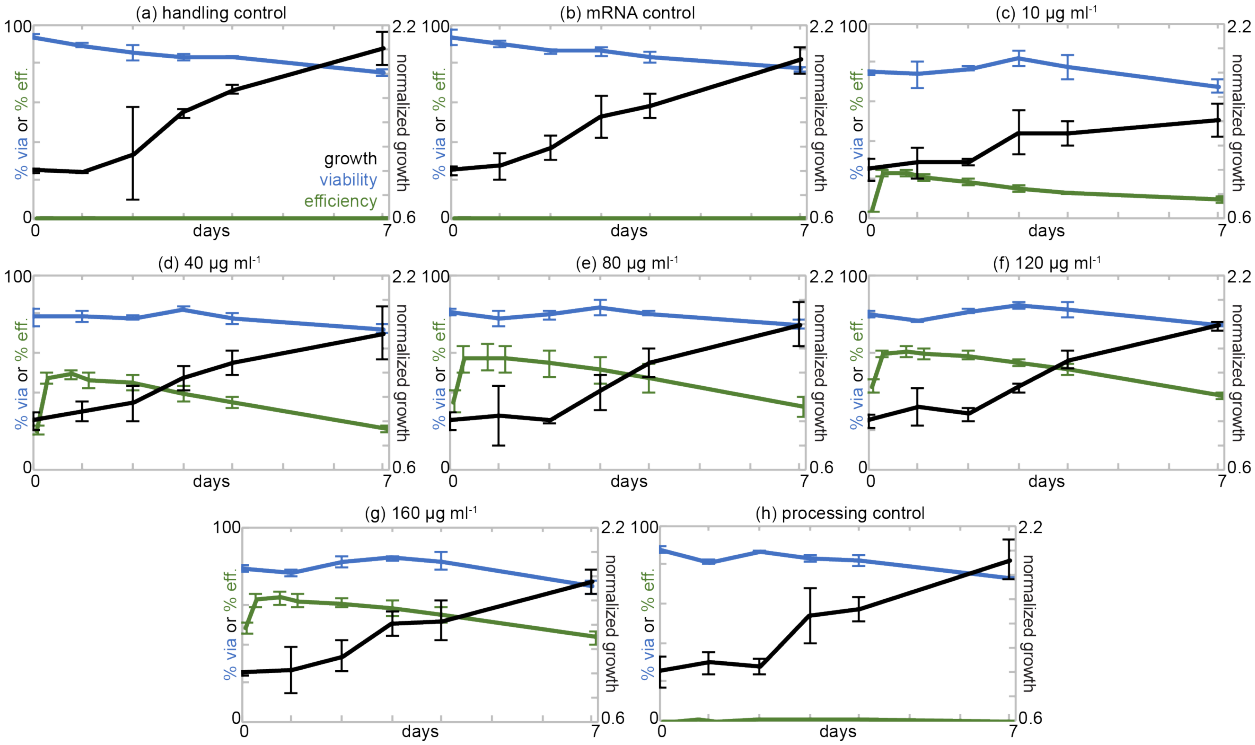

Figure 3 – T cell growth, viability, and EGFP mRNA expression efficiency over 1 week for the (a) handling control, (b) mRNA control, (c) 10 µg mL^{-1}, (d) 40 µg mL^{-1}, (e) 80 µg mL^{-1}, (f) 120 µg mL^{-1}, (g) 160 µg mL^{-1} and (h) device processed control samples. After transfection and return to culture medium, the cell viability (blue line) and concentration (plotted as fold concentration increase, black line) from each group was monitored using trypan blue dye exclusion and an automated cell counter in triplicate. EGFP expression and persistence was quantified using flow cytometry at different time points after transfection. The resulting plots demonstrate that cell growth rate and viability was not adversely affected from on chip mRNA transfection using *µVS*. All groups demonstrated a 2x increase in concentration from post processing growth, except the 10 µg mL^{-1} group, which may have undergone extra stress due to spending the longest time on ice between processing and recovery. Additionally, the persistence of EGFP protein was monitored (green line) and appeared to decrease in signal due to cell growth and protein degradation.

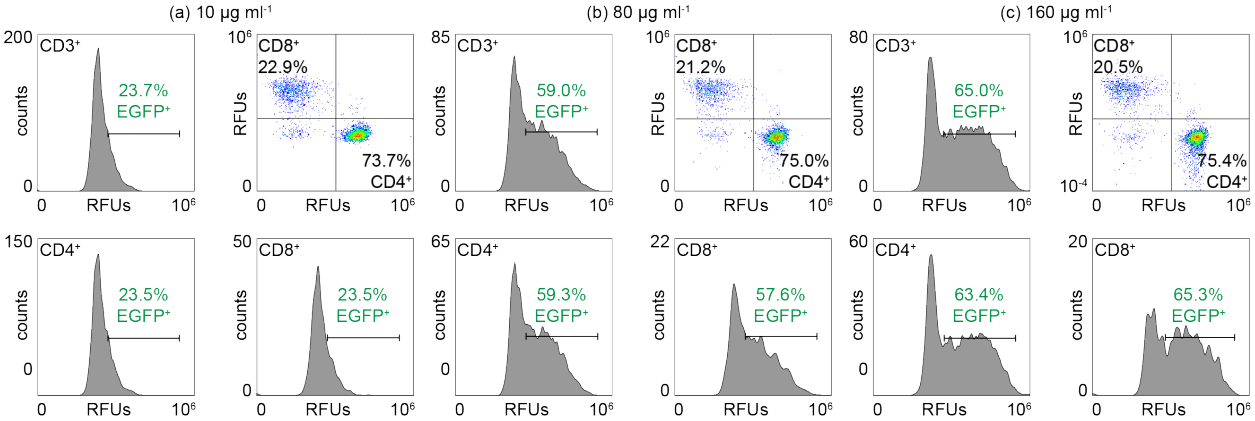

Figure 4 - EGFP expression is equally distributed between the two types of CD3+ cells. *µVS*-based mRNA delivery results in even distribution of expression among the CD8 and CD4 T cells, which is equal to that of the whole CD3+ population EGFP expression. The percentage of CD3+ cells expressing EGFP (upper left histogram) translates to the specific CD4 and CD8 T cell groups (bottom left and right histograms respectively), which were distinguished using fluorescent labeled antibodies (upper right scatter plot), demonstrating no bias for mRNA delivery for helper or cytotoxic T cells. EGFP positive percentages are shown for (a) 10 µg mL^{-1}, (b) 80 µg mL^{-1}, and (c) 160 µg mL^{-1}.

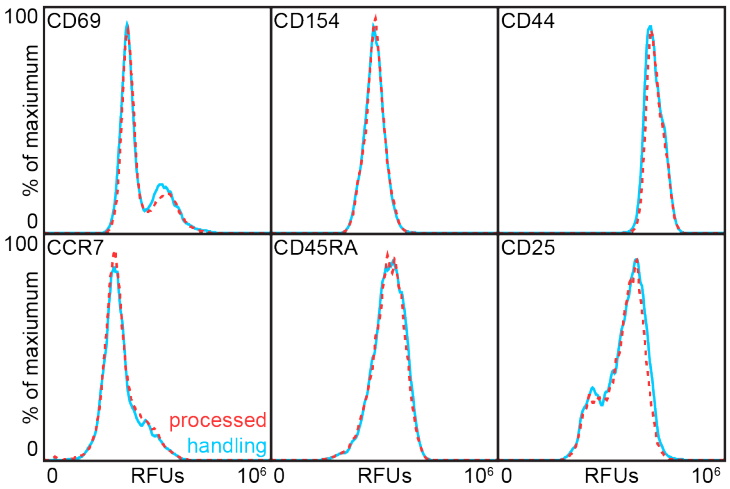

Figure 5 – Overview of the T cell activation profile. After processing and 24 h of cell culture, each replicate from the handling control and processing control were individually labeled with fluorescent antibodies against markers of activation (CD69, CD154, CD44, CCR7, CD45RA and CD25) to assess if *μVS* exposure causes a change in T cell activation state. Replicates from each of the processed control cell and handling control cell group were plotted using FlowJo and the histogram data was overlaid. For all groups, the activation marker expression remained the same between control and device processed groups. Representative overlays of the flow cytometry data are plotted above with the processed control shown in dashed red and the handling control shown in blue. Based on the overlaid data, the activation state and activation/naivety marker expression of pan T cells is not altered because of processing via *μVS*.